Buildings & Cities

Temporal characteristics-based urban heat island effect assessment

RESEARCH

RAJAN RAWAL
SUBHAM DAS
MINU AGARWAL
TEJ CHAVDA
MEGH SHAH
STUTI BANERJEE
BENJAMIN HICKMAN
R. SHANTHI PRIYA

*Author affiliations can be found in the back matter of this article

ubiquity press

ABSTRACT

Urban heat island effect (UHIE) assessments support heat reduction and climate-responsive strategies by informing urban planners, urban designers and local city administrations. Conventional UHIE assessments commonly rely on satellite-derived land surface temperature (LST) to identify hotspots, implicitly treating these locations as thermally representative across intra-day observation periods and seasons. To evaluate this assumption, the temporal characteristics of LST-identified hotspots across the Chennai Metropolitan Area of Tamil Nadu, India, were assessed using one year of field-based air-temperature observations collected from 100 locations representing heterogeneous urban morphology. The assessment analysed thermal hierarchy, thermal-state transitions, persistence and long-term rankings. The results reveal substantial intra-day variability in localised UHIE. The relative thermal hierarchy changed across the morning, afternoon and evening observation periods. Nearly all locations exhibited volatility in their thermal state in at least 25% of observations, while 25% exhibited volatility in more than 50% of observations. Long-term hotspot rankings derived from LST, air temperature and thermal persistence showed limited agreement. More than one-third (36%) of locations identified as hotspots by mean daytime LST were not identified by any other indicator. These findings demonstrate that thermal persistence constitutes an essential dimension of UHIE assessment which supports a more dynamic understanding beyond static LST-based hotspot mapping.

PRACTICE RELEVANCE

In 2019, under Section 18(2) of the Disaster Management Act, 2005, of the Government of India, the National Disaster Management Authority (NDMA) laid down guidance on prevention, mitigation and preparedness for heatwaves. As part of this framework, local city administrations are requested by the NDMA to prepare 'heat action plans' (HAPs). The UHIE assessment forms an integral component of these HAPs. Current UHIE assessments

CORRESPONDING AUTHOR:
Rajan Rawal
CEPT University, Kasturbhai Lalbhai Campus, University Road, Navrangpura, Ahmedabad—380009, IN
rajanrawal@cept.ac.in

KEYWORDS:
urban heat island; urban microclimates; thermal persistence; land surface temperature (LST); canopy-layer urban heat island (CLUHI); air temperature; heat action plans; cities; India

TO CITE THIS ARTICLE:
Rawal, R., Das, S., Agarwal, M., Chavda, T., Shah, M., Banerjee, S., Hickman, B., & Shanthi Priya, R. (2026). Temporal characteristics-based urban heat island effect assessment. *Buildings and Cities*, 7(1), pp. 1375–1396. DOI: https://doi.org/10.5334/bc.901

primarily rely on satellite-derived LST-based hotspot identification. This approach does not capture the temporal characteristics of localised UHIE. This study demonstrates that incorporating thermal persistence alongside conventional thermal indicators enables practitioners to distinguish persistently hot locations from transient hotspots. This additional temporal dimension can strengthen the prioritisation of heat-mitigation interventions and support more targeted investigation of the factors contributing to localised heat stress in rapidly urbanising cities.

1. INTRODUCTION

Urbanisation has transformed India's built environments and positioned cities as key drivers of socio-economic development (NITI Aayog & Asian Development Bank 2022). Between 1990 and 2015, India's urban land area increased by 74% from approximately 98,800 to 171,839 km^2. During the same period, the extent of the building footprint increased by 79%, from 17,505 to 31,456 km^2 (Pesaresi & Politis 2023; World Bank 2026). These transformations replaced natural and pervious surfaces with dense impervious built cover and altered the surface energy balance of cities (Grimmond & Oke 1999; Oke 1982). As a result, the urban heat island effect (UHIE) has emerged as a major concern, especially during extreme heat events, due to its impact on pedestrian heat stress, operational energy demand and heat-related health risks (Islam *et al.* 2024; Kumari *et al.* 2021; Mandvikar *et al.* 2024). The National Disaster Management Authority (NDMA) (2019) stresses that India's heatwaves are becoming more frequent and intense, making effective management imperative to lower heatwave-linked mortality and protect economic productivity.

These concerns are pronounced in the Chennai Metropolitan Area (CMA) of Tamil Nadu, India. Among the top 37 Class I cities in India (with a population > 100,000), Chennai recorded the highest heat-health vulnerability based on geospatial and demographic indicators (Mandvikar *et al.* 2024). Long-term projections also positioned Chennai with the highest probability (98.2%) of strong heat stress in summer (Kumar *et al.* 2022). The city experienced 42 heatwave-days during the period 1985–2014, and is projected to record 81 heatwave-days annually during the period 2021–50 (Anna University 2024a). Moreover, annual thermal discomfort-days are also projected to increase from approximately 100–125 during the period 1985–2014 to 200–250 during 2021–50 (Anna University 2024b). Projections under a high-emissions scenario suggest a 30–50% increase in extremely hot days and nights by 2050 across dense neighbourhoods of Chennai (World Bank 2025), underscoring the need for a targeted heat mitigation approach.

This study addresses two types of urban heat islands (UHI), the surface urban heat island (SUHI) and the canopy-layer urban heat island (CLUHI) (WMO 2023). The SUHI is the difference in surface temperature between urban and rural areas. It is derived from the radiometric temperature of surfaces observed by thermal remote sensing and generally reaches its maximum during daytime (Voogt & Oke 2003; WMO 2023). The CLUHI is the excess of near-surface air temperature in urban areas over their rural surroundings, typically measured at 1.25–2.00 m above ground within the urban canopy layer, and is most pronounced at night (WMO 2023). The SUHI and CLUHI differ in physical basis, magnitude and temporal behaviour (Du *et al.* 2023; Sun *et al.* 2020).

In UHIE studies, a hotspot or heat sink refers to a geographical location with elevated or sunken thermal conditions relative to the surrounding urban environment. Existing studies primarily rely on remote sensing for identifying hotspots and heat sinks from satellite-derived land surface temperature (LST), and only a few studies validate these findings through field observations (Islam *et al.* 2024; Mohan *et al.* 2022; Sharma *et al.* 2026). Field observations primarily include air temperature to assess localised CLUHI (Kotharkar *et al.* 2018; Mohan *et al.* 2022). A global review of 778 remote sensing-based UHIE studies published between 1978 and 2018 reported that almost 69% of the studies relied on observations from a single time of day. Daytime LST accounted for 63% of the studies, while only 23% looked at seasonal variability (Zhou *et al.* 2019). Reliable hotspot identification is essential for heat-mitigation prioritisation and climate-responsive city planning and governance.

However, the temporal behaviour of hotspots remains insufficiently understood. Empirical studies report temporal variability in both LST- and air temperature-based UHI characteristics, including inconsistencies in daily, weekly and seasonal trends. Thermal persistence has been studied less frequently than hotspot magnitude, particularly using field observations (Li *et al.* 2024a). Variability in the thermal characteristics of a hotspot was observed between remote sensing and *in-situ* field observations (Acosta *et al.* 2023; Du *et al.* 2023). These findings suggest that the satellite-derived LST alone may not adequately represent the spatial and temporal variability of localised UHIE (Zhan *et al.* 2025). In this study, satellite-derived LST is used to identify and rank representative hotspots and heat sinks, and repeated near-surface air-temperature observations from *in-situ* field campaigns are used to evaluate their temporal behaviour in the urban canopy layer.

1.1 BACKGROUND

1.1.1 Overview of remote sensing-based surface UHI assessments

Remote sensing-based SUHI assessments primarily analyse satellite-derived LST together with land-use land-cover (LULC) and spectral metrics such as the normalised difference vegetation index (NDVI) (Peng *et al.* 2012; Weng 2009). Review studies across Indian cities report mean day- and night-time LST-based UHI intensity differences (ΔUHI) of 5–8 and 1–5°C, respectively (Islam *et al.* 2024; Kotharkar *et al.* 2018; Rajagopalan 2021).

Satellite observations represent radiometric surface temperature, rather than near-surface air temperature (Li *et al.* 2023; Sun *et al.* 2020; Voogt & Oke 2003). This difference limits the representation of localised CLUHI dynamics (Yang *et al.* 2024; Zhan *et al.* 2025; Zhou *et al.* 2019). Reported differences between satellite-derived LST and field-measured air temperature range from −7 to more than 30°C, depending on land cover, urban morphology, micrometeorological conditions and observation time (Anniballe *et al.* 2014; Ho *et al.* 2016; Naserikia *et al.* 2023; Zhao *et al.* 2026). Microclimate studies observed peak night-time heat stress in narrow street canyons despite observing moderate daytime LST (Chatzidimitriou & Yannas 2017; Lee *et al.* 2026).

Satellite sensor characteristics also influence UHIE mapping and assessment. Spatial resolution, thermal radiation directionality, revisit frequency and satellite overpass time affect the representation of urban thermal patterns (Almeida *et al.* 2021; Sobrino *et al.* 2012; Wang *et al.* 2022). Differences in spatial resolution, acquisition timing, and grid alignment introduce challenges in hotspot identification and data analysis (Zhao *et al.* 2025; Zhou *et al.* 2019). For example, the coarse spatial resolution of the Moderate Resolution Imaging Spectroradiometer (MODIS) sensor aggregates thermally heterogeneous urban surfaces within a single 1-km pixel (Branea *et al.* 2016). This subpixel blending introduces systematic averaging errors because thermal radiance is non-linearly linked to surface temperature, limiting the interpretability of pixel-scale LST relevant to hotspot identification (Kustas & Norman 2000; Stumpe *et al.* 2026; Zhao *et al.* 2025). Field validation of intra-urban UHIE variability (Briegel *et al.* 2025; Naserikia *et al.* 2023) and hotspot persistence (Magyari-Sáska *et al.* 2024) also remains limited.

1.1.2 Overview of field observation-based canopy layer UHI assessments

In-situ field observations measure microclimatic conditions at regular intervals to characterise CLUHI (Acosta *et al.* 2023; Johansson *et al.* 2014; Lefevre *et al.* 2026). Transect surveys such as mobile traverses are widely adopted for mapping spatial thermal gradients across heterogeneous urban environments (Jaiswal *et al.* 2023; Martinez-Soto *et al.* 2025; Muller *et al.* 2013a). Hotspot identification methods and instrumentation strategies for field campaigns are established in urban climate research (Rawat & Singh 2022; Sharma *et al.* 2026). Observational studies in tropical cities reveal significant intra-urban thermal variability driven by urban morphology (Huang & Wang 2019; Jaiswal *et al.* 2023). Field observations, together with numerical modelling, also capture night-time heat retention within street canyons (Chatzidimitriou & Yannas 2017; Oke 1981). Therefore, *in-situ* observations provide an important and additional reference for evaluating the representativeness and reliability of LST-derived hotspots and heat sinks.

Field surveys across Indian cities report substantial intra-day variability in air temperature. During daytime, urban–rural air temperature contrasts are generally lower, with afternoon UHI intensities (ΔT_{air}) commonly ranging between 3 and 4°C (Mohan *et al.* 2022). In contrast, night-time intensities are more pronounced, ranging between 1.5 and 5°C. Review studies indicate that seasonal mean UHI intensities can range between 2.0 and 10.3°C, particularly in dense areas (Islam *et al.* 2024; Mohan *et al.* 2022; Rajagopalan 2021). Moreover, local climate zone (LCZ)-based studies reported air temperature differences ranging between 1.76 and 4.09°C during the morning period across different built forms, with compact low-rise neighbourhoods exhibiting higher heat accumulation (Kotharkar & Bagade 2018). These findings highlight the importance of field observations for assessing the microclimate (Lefevre *et al.* 2026).

However, they are constrained by limited monitoring locations, shorter observation periods and instrument accuracy over time. Moreover, high deployment costs, intensive logistics and limited spatial coverage challenge spatially synchronous observations across heterogeneous urban environments (Muller *et al.* 2013b; Santamouris 2015). These practical constraints limit the spatial and temporal representativeness achieved by individual field campaigns.

1.1.3 Knowledge gap

Prevalent UHIE assessments are commonly derived from temporally discrete observations, while repeated field observations describing hotspot behaviour across multiple observation periods remain limited (Kim & Brown 2021; Shi *et al.* 2021). Recent studies indicate that the relationship between LST and air temperature is highly context dependent, limiting the reliability of LST-derived hotspots (Li *et al.* 2024b; Schwarz *et al.* 2011). Strong agreement between mean LST- and air temperature-based UHIE estimates ($R^2 = 0.794$) has also been accompanied by opposite temporal trends in 54% of cities for minimum night-time temperatures and of 38% for maximum daytime temperatures. These findings indicate that LST-derived hotspots may not reliably represent persistent heat stress (Sun *et al.* 2020).

Indian cities provide a relevant context to study the impact of urbanisation, anthropogenic heat emissions and tropical meteorological conditions on UHIE (Islam *et al.* 2024; Mohan *et al.* 2022). Uncertainty in hotspot identification limits the identification of key factors of UHIE and their consequences for planning and mitigation decisions. Therefore, assessing both the spatial and temporal characteristics of UHIE is essential for an evidence-based framework for Indian cities.

To identify ground locations for ground measurements, this study initially employs LST to identify thermal hotspots. The results reinforce literature findings that LST mapping alone cannot fully capture ground reality (Briegel *et al.* 2025; Naserikia *et al.* 2023; Sun *et al.* 2020; Venter *et al.* 2026). Consequently, the paper bridges this critical research gap with two major findings: first, it confirms the inadequacy of standalone LST hotspot identification; and second, it demonstrates temporal variability, showing that hotspot rankings fluctuate across days, weeks and months, which proves that the hottest locations do not remain static over time.

1.2 AIM AND OBJECTIVES

This study evaluates the reliability of the satellite-derived LST-based hotspot identification approach for UHIE assessment by examining the temporal characteristics of identified locations called hotspots. Set in the CMA, the study analyses the temporal behaviour of LST-derived hotspots using repeated field-based air-temperature measurements collected over one year. The assessment examines intra-day thermal hierarchy, thermal-state transitions, persistence, volatility and long-term hotspot rankings.

2. METHODS

2.1 STUDY CONTEXT

The study was conducted in the Chennai Metropolitan Area (CMA), a coastal urban region of the state of Tamil Nadu covering approximately 1189 km² along the Bay of Bengal (13.08°N, 80.27°E). Chennai is classified as a warm-humid climate zone as per the National Building Code

of India (BIS 2016). Mean annual maximum and minimum air temperatures are 32.8 and 24.5°C, respectively, with a mean relative humidity of 76%. May is considered the hottest period in the year (Jeganathan *et al.* 2016).

Between 1991 and 2021, Chennai's built-up area expanded nearly threefold, from 102 to 295 km², while vegetation cover declined from 23% (101.90 km²) to 17% (74.35 km²) (Greater Chennai Corporation *et al.* 2023). From 2001 to 2022, Chennai exhibited an increase in LST-derived SUHI intensity of 0.033°C/year in winter and 0.019°C/year in summer (Gadekar & Mathew 2026). Previous studies in Chennai have focused on hotspot identification, assessing the relationship between LULC and LST, and the influence of urban morphology on outdoor thermal comfort (Kesavan *et al.* 2021; Rajan & Amirtham 2021). However, evidence for the temporal characteristics of the hotspots is limited.

In this study, an LST-based hotspot identification approach was complemented with repeated field-based air temperature measurements to assess their short- and long-term characteristics to provide a comprehensive basis for UHIE assessment and heat-mitigation prioritisation (Figure 1).

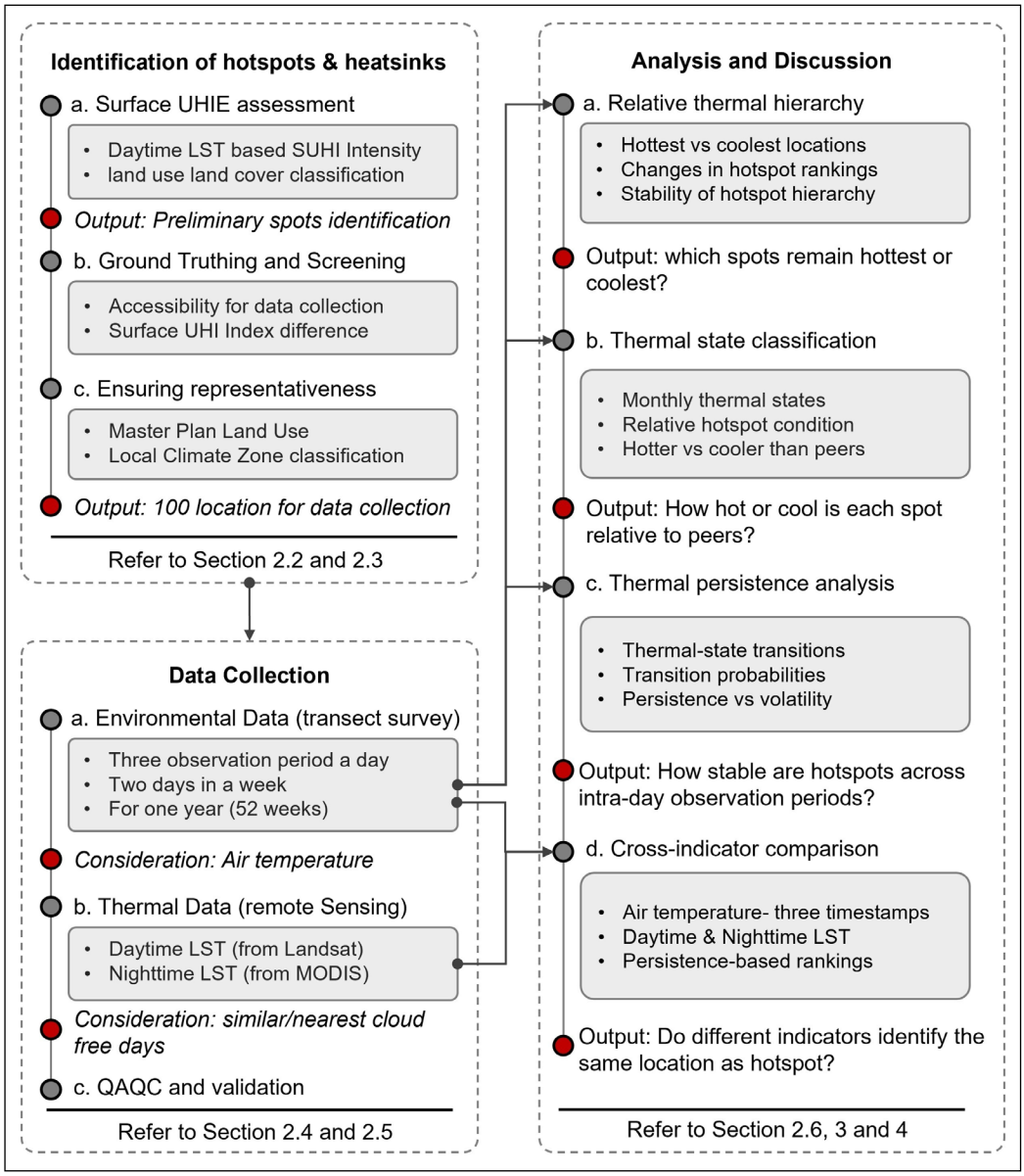

Figure 1: Study process summary.

2.2 IDENTIFICATION OF HOTSPOTS AND HEAT SINKS

The study adopted the identified locations (hotspots and heat sinks) from an existing study (Rajagopal *et al.* 2025), in which daytime LST derived from Landsat 5 TM (14 May 2006) and

Landsat 8 OLI/TIRS (26 May 2022) was used to calculate the UHI index for a 100 × 100 m grid covering the CMA. Locations were initially sorted by UHI index difference (2006–22) and then screened by replicating the actual percentage distribution of each land-use category from the master plan (Figure 2). After the field validation, it provides background to this present study by deriving a composite scoring index based on site accessibility for data collection and the UHIE index difference. To reduce spatial sampling bias and better capture the spatial heterogeneity of the urban thermal environment across the CMA, this study refined the final selection of locations for the *in-situ* field observations. To ensure good geographical distribution, 90 hotspots and 10 heat sinks were finalised for *in-situ* field observations (Figure 3A).

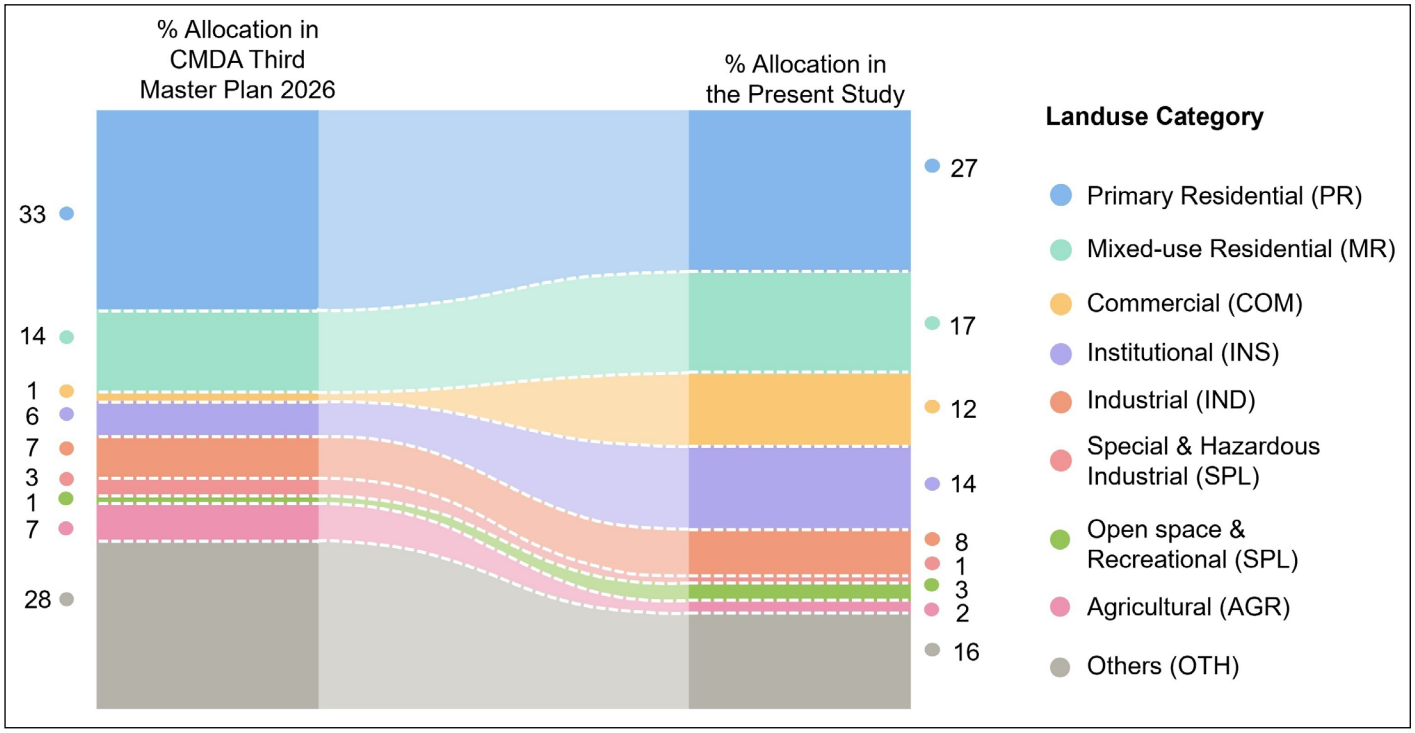

Figure 2: Distribution of land-use categories of the Chennai Metropolitan Area (CMA) and their correspondence with selected hotspots and heat sinks. *Source:* Adapted from CMDA (2008).

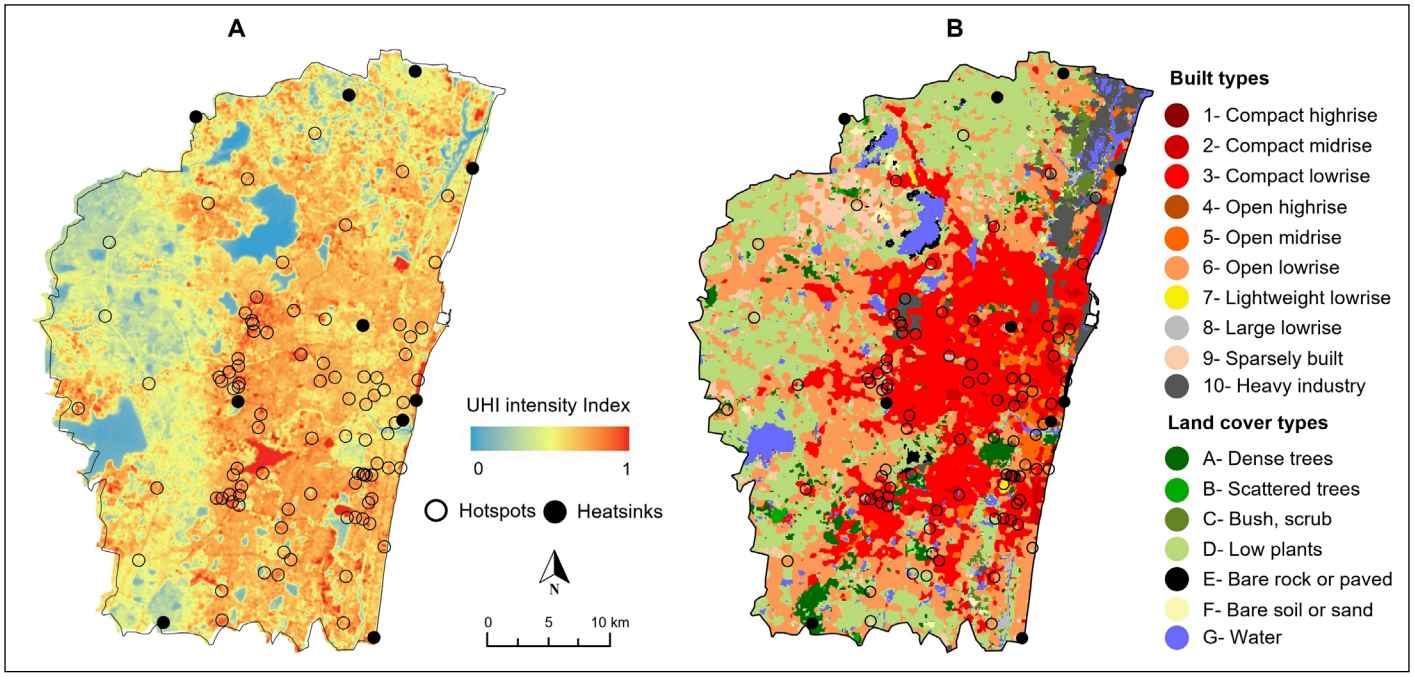

Figure 3: Chennai Metropolitan Area (CMA): **(A)** land surface temperature (LST)-based urban heat island effect (UHIE) assessment showing the study locations; and **(B)** local climate zone (LCZ) classification.

2.3 LCZ CLASSIFICATION

The LCZ classification was performed in the urban morphological context in order to interpret the observed thermal behaviour (see Section 4). It was generated for 2025 using the WUDAPT LCZ Generator (Demuzere *et al.* 2021). Classification was carried out at 100 m spatial resolution following the LCZ framework that comprises 10 built-type classes and seven natural land-cover classes (Stewart & Oke 2012). The LCZ map (Figure 3B) was produced using the WUDAPT workflow, which employs a random forest (RF) machine-learning classifier within the Google Earth Engine (GEE) environment (Bechtel *et al.* 2015). Figure 4 illustrates the distribution of LCZ classes and their corresponding land-use categories across the 100 representative locations in CMA.

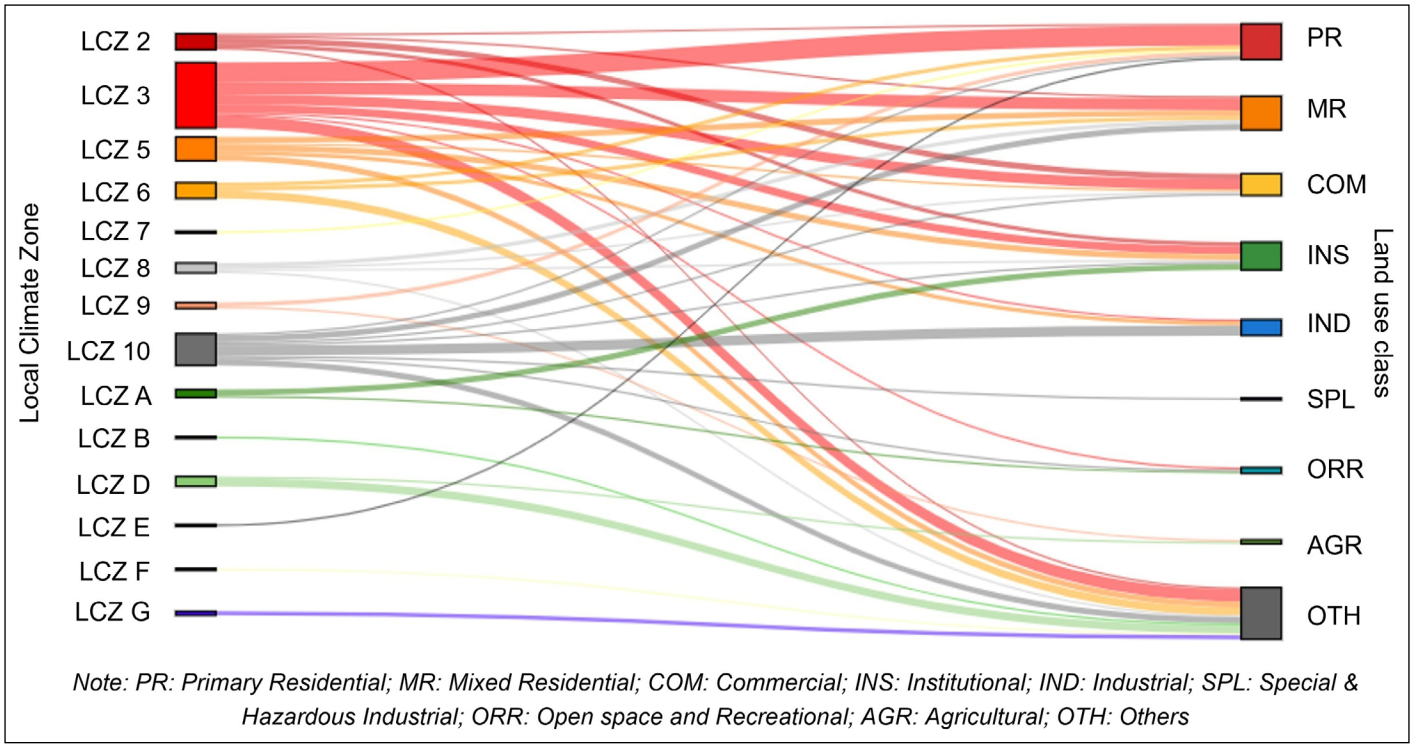

Figure 4: Distribution of local climate zone (LCZ) types and their corresponding land-use categories identified in the Chennai Metropolitan Area (CMA).

Note: PR = primary residential; MR = mixed residential; COM = commercial; INS = institutional; SPL = special and hazardous industrial; ORR = open space and recreational; AGR = agricultural; OTH = others.

2.4 DATA COLLECTION

2.4.1 Field measurements

Field observations were conducted using 11 mobile traverse routes covering the study locations to measure the environmental parameters. The traverses were designed in accordance with the WMO's *Guide to Instruments and Methods of Observation* (2024), facilitating broad spatial coverage. Traverse lengths and travel durations were optimised according to route extent to minimise temporal inconsistencies between observation periods. Measurements were collected twice a week over one year (1 September 2023–31 August 2024) across three periods: 08:00–12:00 hours (morning), 13:00–17:00 hours (afternoon) and 18:00–22:00 hours (evening). This sampling strategy captured both intra-day and seasonal variations in the localised thermal environment. The study locations with one sample transect route and their measurement protocol are shown in Figure 5.

Air temperature (°C), relative humidity (%) and globe temperature (°C) were measured using an Extech HT200 heat stress meter. Wind speed (m/s) and surface temperature (°C) were measured using a Testo 410-2 vane anemometer and a Fluke Ti32 infrared thermal camera, respectively. Air temperature was adopted as the primary variable in the scope of this study (Kotharkar *et al.* 2018; Mohan *et al.* 2022). For a summary of the campaign, consisting of the observation period, duration and instrument, see Table 1.

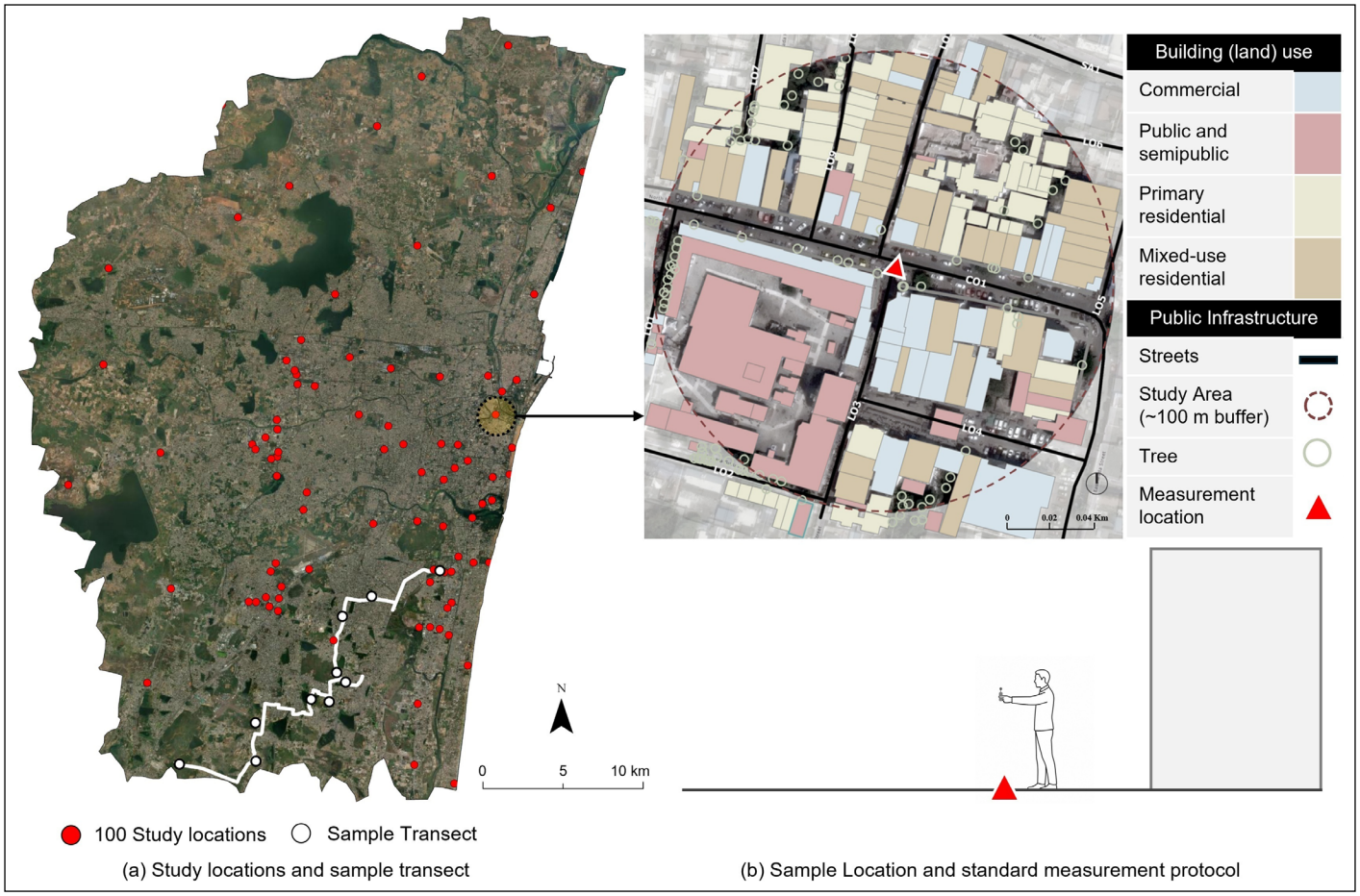

Figure 5: (a) Study locations across the Chennai Metropolitan Area (CMA) and sample transect (shown in white); and **(b)** sample location and measurement protocol.

CAMPAIGN DETAILS	
Campaign duration and period	1 year (September 2023–August 2024)
Study locations	100 locations
Transect design	11 transects (routes) covering all 100 locations
	Transect duration: 1–2 h
Observation schedule of each transect	Measurement frequency: 2 days/week
	Daily observation period: morning (08:00–12:00 hours), afternoon (13:00–17:00 hours) and evening (18:00–22:00 hours)

MEASURING INSTRUMENTS DETAILS				
Measured parameter (units)	**Instrument/sensor specification**	**Measurement range**	**Resolution**	**Accuracy**
Air temperature (°C)	Extech HT200 heat stress meter	0–50	0.1	±0.8
Relative humidity (%)		1–99%	0.1%	±3%
Globe temperature (°C)		0–80	0.1	±0.6
Wind speed (m/s)	Testo 410-2 vane anemometer	0.4–20.0	0.1	± (0.2 m/s + 2% of measured value)
Surface temperature (°C)	Fluke TiR32 infrared camera	–20 to +150	n.a.	±2°C or ±2% of reading

Table 1: Summary of the measurements.

Note: Only air temperature measurements are considered, corresponding to the objective of the study.

2.4.2 Satellite-derived thermal datasets

To compare long-term hotspot rankings derived from field-based air temperature with satellite observations, day- and night-time LST datasets were obtained from the Landsat 8/9 series and MODIS (Terra), respectively. Landsat 8/9 provides daytime LST acquisitions at approximately 10:30 IST (India standard time) with an effective eight-day revisit interval and a native thermal infrared (TIR) spatial resolution of 100 m. Raster values at each study location were sampled to extract LST from both datasets (Zhou *et al.* 2019).

Although the study surveyed 11 traverse routes twice a week, observations at individual study locations did not always occur on the same day. Moreover, to account for the revisit interval, a retrospective temporal matching approach was adopted using the most recent Landsat acquisition preceding each field observation (Figure 6A):

- *Scenario 1:* if a field observation coincided with a cloud-free Landsat acquisition (days 1, 9 or 17), the LST value from the same date was used (6% of the total samples; $n = 2743$).
- *Scenario 2:* if a field observation fell between two acquisition dates (days 2–8), the LST value from the previous cloud-free acquisition (day 1) was used (42%).
- *Scenario 3:* if the day 9 acquisition was unavailable because of cloud cover, observations collected between days 9 and 16 were matched with the previous cloud-free acquisition (day 1) (28%).
- *Excluded observations:* field observations were excluded if no cloud-free image was available within the representative acquisition period (24%).

Night-time LST was obtained from MODIS (Terra), which provides daily observations at approximately 22:30 IST with a spatial resolution of approximately 1 km. LST values were extracted from the same date as the field observations or, where unavailable because of cloud cover, from the nearest cloud-free acquisition. Owing to the coarser spatial resolution, multiple study locations intersected the same MODIS pixel and therefore shared identical night-time LST values, whereas Landsat distinguished these locations using separate daytime LST values (Figure 6B). Considering these temporal and spatial constraints (Stumpe *et al.* 2026; Zhao *et al.* 2025; Zhou *et al.* 2019), only the 86 study locations with complete datasets were included in the long-term hotspot ranking analysis (see Section 3.4) to minimise bias associated with incomplete observations.

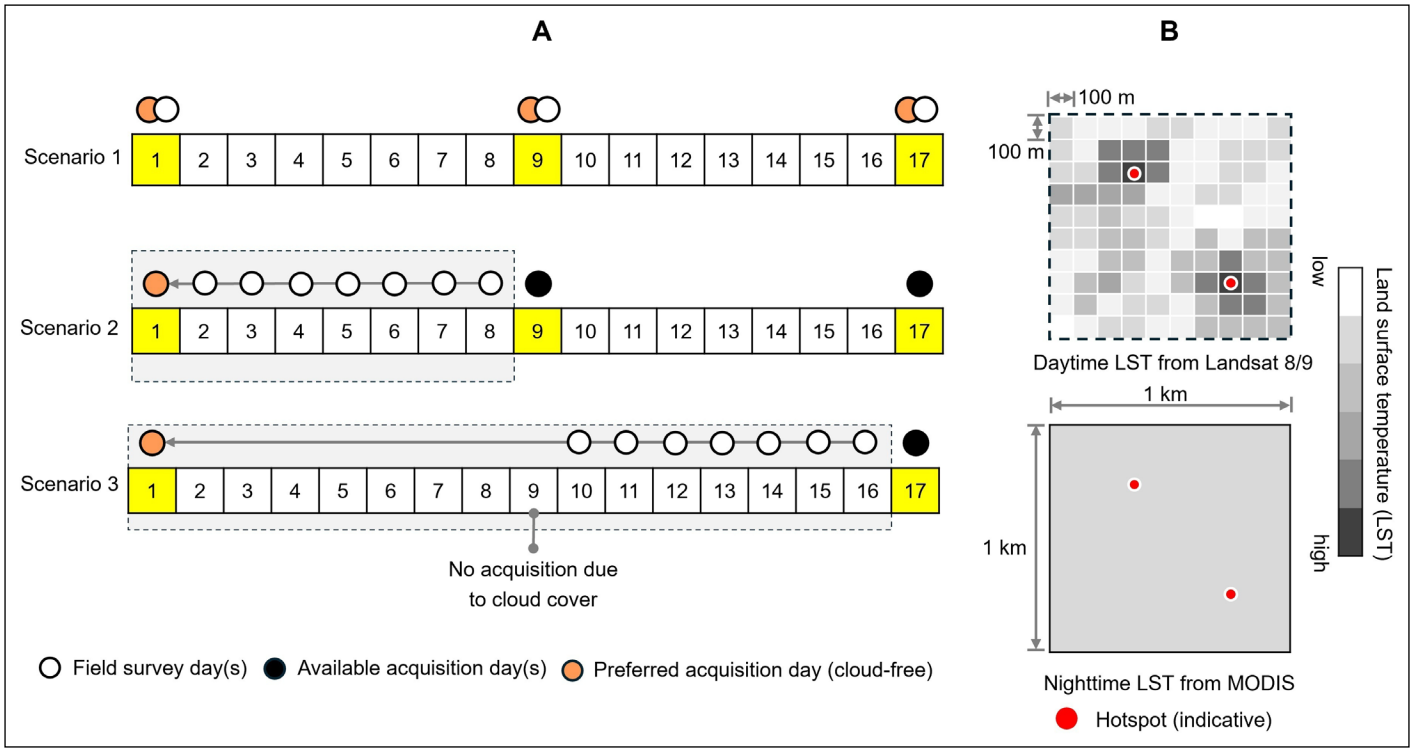

Figure 6: (A) Temporal matching of Landsat 8/9 daytime acquisitions; and **(B)** comparison of Landsat (100 m) and MODIS (1 km) spatial resolutions, showing two distinct hotspots identified from daytime land surface temperature (LST) correspond to an identical night-time LST value, limiting the assessment.

2.5 DATA QUALITY CONTROL AND VALIDATION

Measurement instruments were calibrated before field deployment. Raw observations underwent quality control to remove records affected by rainfall, instrument malfunction, incomplete traverses or recording errors. Statistical outliers were identified using the 1.5× interquartile range (IQR) criterion, and monthly distributions were examined using descriptive statistics (minimum, maximum, mean, standard deviation) to identify anomalous observations. Data completeness was evaluated for each study location, month and observation period to ensure consistent temporal coverage across the monitoring period. Following quality control, the screened dataset was compared with long-term (1970–2023) air-temperature records from the India Meteorological Department (IMD) observatories at Nungambakkam and Meenambakkam to verify that the observations remained within the expected intra-day and seasonal variances.

2.6 ANALYSIS

The analytical framework evaluated the temporal behaviour of the study locations using field-based air-temperature observations and satellite-derived LST data. It distinguishes between short- and long-term thermal dynamics derived from repeated observations. Five analytical concepts underpin the analyses:

- Thermal groups are eight ordinal categories (groups 0–7) defined according to the deviation of air temperature from the monthly mean (m) and standard deviation (s). Groups 0–3 represent hotter-than-peer conditions, whereas groups 4–7 represent cooler-than-peer conditions.
- A thermal state represents the relative thermal condition of a location during a given month and observation period. Each location was assigned to one of the eight thermal groups, enabling comparison of its thermal condition with that of its peers under comparable seasonal and intra-day conditions.
- A transition represents a change in thermal state between consecutive observation periods (morning to afternoon and afternoon to evening). Transition probabilities were estimated using 8 × 8 Markov transition matrices.
- Persistence and volatility describe the stability and change in thermal state across successive observation periods. Persistence represents the tendency of a location to remain within the same thermal domain, whereas volatility represents transitions between hotter- and cooler-than-peer domains. Both metrics were derived from the Markov-chain transition probabilities.
- Rank defines the long-term thermal hierarchy of monitored locations based on their repeated tendency to exhibit higher thermal dominance than their peers over the study period. Unlike thermal state, which describes the thermal condition during a single observation period, rank summarises the long-term thermal behaviour of a location. Rankings were derived independently for each thermal indicator, and agreement among the indicator-specific rankings was visualised using an UpSet plot.

Based on these analytical concepts, the framework comprised four sequential stages:

- Evaluation of temporal variation in the thermal hierarchy.
- Thermal-state classification.
- Analysis of thermal-state transitions, persistence and volatility.
- Comparison of hotspot rankings derived from different thermal indicators.

2.6.1 Temporal variation in the thermal hierarchy

The first stage of the analysis examined temporal variation in the thermal hierarchy across the three daily observation periods. For each period (*e.g.* morning, afternoon and evening), the mean air temperature of each study location was calculated from all field observations collected during

the study period (1 September 2023–31 August 2024). Study locations were ranked from the highest to the lowest mean air temperature for each observation period (Figure 7). Comparison of the resulting thermal hierarchies described temporal variation in localised UHIE and informed the subsequent thermal-state classification.

2.6.2 Thermal-state classification

The second stage classified each air-temperature observation into one of eight thermal groups based on its deviation from the monthly mean air temperature and standard deviation. For each month and observation period, the mean air temperature (m) and standard deviation (s) were calculated using observations from all 100 study locations. Each observation was assigned to one of eight thermal groups according to its deviation from m (Table 2). Group 0 represents observations exceeding m + 1.5 s, and group 7 includes observations below m – 1.5 s. Groups 0–3 represent hotter-than-peer states and groups 4–7 represent cooler-than-peer thermal states. The corresponding monthly thresholds are presented in Figure 8.

Percentile-based approaches have frequently been used to delineate urban heat hotspots (Li *et al.* 2026; Sola-Caraballo *et al.* 2025). These approaches classify observations by rank and may not reflect meaningful temperature differences between observations. In this study, the objective was not to delineate physical hotspot boundaries but to evaluate temporal persistence relative to monitored peers. Thermal-group thresholds were therefore derived from the monthly mean air temperature and standard deviation for each observation period. This approach accounts for seasonal and intra-day variation and provides a consistent basis for subsequent analyses.

THERMAL GROUP	AIR-TEMPERATURE THRESHOLD
0 (Hottest)	> m + 1.5 s
1	< m + 1.5 s and > m + s
2	< m + s and > m + 0.5 s
3	< m + 0.5 s and > m
4	< m and > m – 0.5 s
5	< m – 0.5 s and > m – s
6	< m – s and > m – 1.5 s
7 (Coolest)	< m – 1.5 s

Table 2: Air-temperature thresholds used for thermal-state classification.

Note: m = mean; s = standard deviation.

2.6.3 Markov-chain analysis of thermal-state transitions

Transitions in thermal state between consecutive observation periods (morning to afternoon and afternoon to evening) were analysed using a discrete-time, first-order Markov chain. First-order Markov chains provide an established framework for analysing sequential observations classified into a finite set of discrete states, in which the probability of a future state depends only on the current state (Gabriel & Neumann 1962; Katz & Parlange 1998). The Markov-chain framework was used to characterise thermal persistence by quantifying the empirical tendency of study locations to retain or change their thermal state across successive observation periods. The resulting probabilities describe observed thermal behaviour rather than the processes governing UHIE.

An 8 × 8 transition probability matrix was constructed for each study location for the morning to afternoon and afternoon to evening observation sequences (Figure 9). Transition probabilities were estimated from the observed frequencies of movement between thermal groups (Wilks 2011). Rows represent the thermal group during the earlier observation period, and columns represent the subsequent thermal group. Each matrix element represents the probability of transition between the corresponding groups. For example, the element group 6 (morning) to group 6 (afternoon) represents the probability that a location classified in group 6 during the morning remained in group 6 during the afternoon. The principal diagonal therefore represents thermal persistence, whereas off-diagonal elements represent transitions between thermal groups, reflecting thermal volatility.

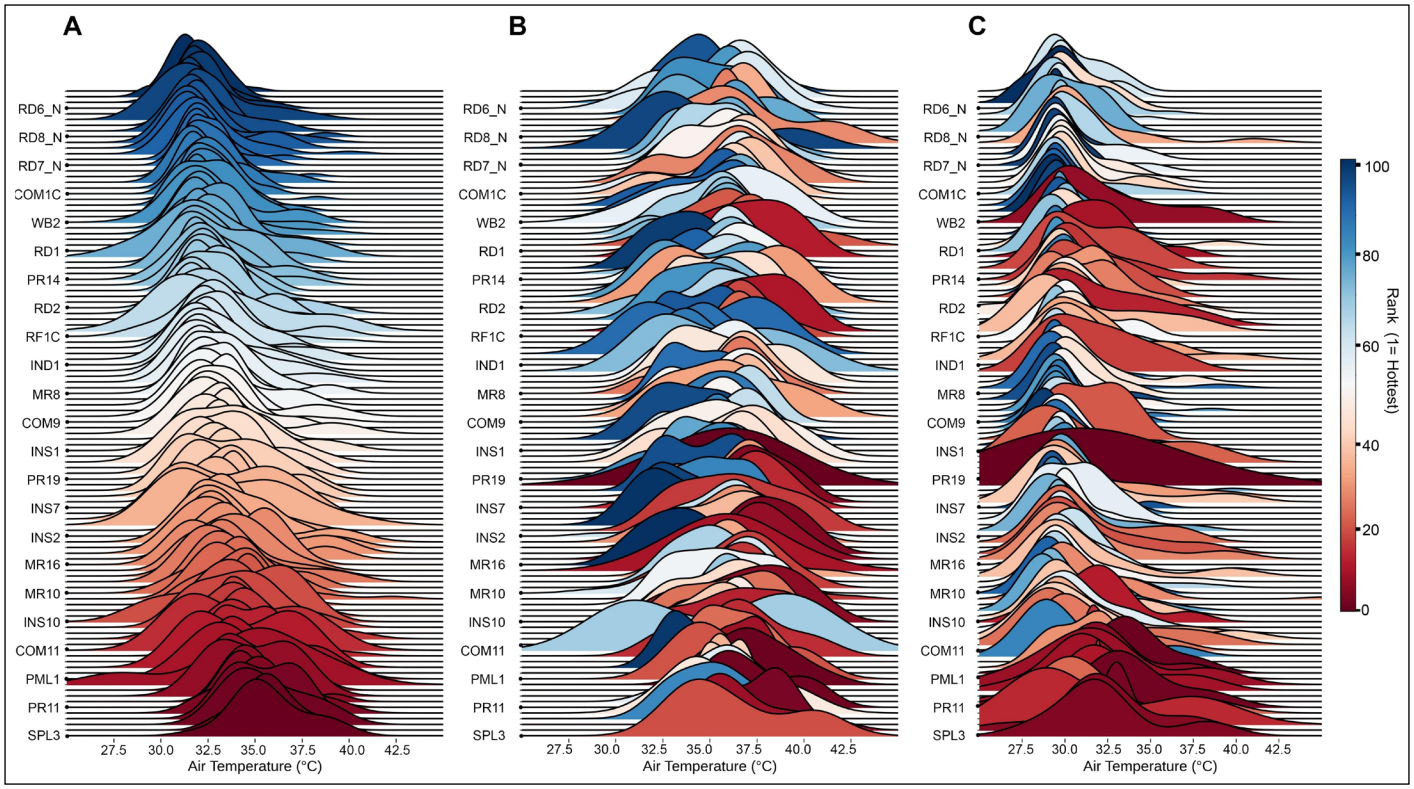

Figure 7: Mean air temperature distribution across 100 study locations in the Chennai Metropolitan Area (CMA) (1 September 2023–31 August 2024) during **(A)** morning, **(B)** afternoon and **(C)** evening observation periods.

Note: Colours indicate the thermal rank of each location, with rank 1 representing the hottest location.

Persistence and volatility were quantified from transitions within and between the hotter- and cooler-than-peer thermal domains. Persistence was calculated as the proportion of transitions remaining within the same domain, and volatility as the proportion between domains. Transitions involving groups 3 and 4 were excluded because these groups lie adjacent to the monthly mean air temperature and do not represent meaningful shifts between hotter- and cooler-than-peer conditions (Figure 10). The resulting metrics were subsequently used as an independent thermal indicator in the hotspot ranking analysis.

2.6.4 Variability in hotspot rankings across thermal indicators

Independent hotspot rankings were derived from mean air temperature, day- and night-time mean and maximum LST, and thermal persistence (see Section 2.6.3). For each indicator, study locations were ranked independently, with rank 1 assigned to the location exhibiting the highest value. Agreement among the indicator-specific rankings was visualised using an UpSet plot. Study locations were considered to agree if their rankings differed by no more than ±5 positions. For the 100 ranked study locations, this corresponds to a maximum allowable rank displacement of 10 positions (approximately 10% of the ranking), adopted as an operational tolerance to accommodate minor ordinal differences between ranking methods. Locations satisfying this criterion were assigned to the corresponding intersection, whereas the remaining locations were assigned to indicator-specific intersections.

In the UpSet plot, rows represent thermal indicators and columns represent unique intersections among hotspot rankings (Figure 11). Connected filled circles identify the contributing indicators, vertical bars indicate the number of study locations in each intersection and horizontal bars indicate the total identified by each indicator.

3. RESULTS

3.1 TEMPORAL VARIATION IN THE THERMAL HIERARCHY

The thermal hierarchy of the study locations varied across the three observation periods (Figure 7). Rank reordering was greatest between the morning and afternoon observations and remained evident during the evening. Changes occurred primarily among intermediate-ranked locations; however, the warmest and coolest locations remained comparatively stable.

SPL3 (Pallavaram) and PR11 (Tharamani) consistently ranked among the warmest locations. RD6_N (Manali New Town), RD7_N (Vadaperumbakkam) and RD8_N (Palanjur) remained among the coolest across all observation periods. In contrast, intermediate-ranked locations showed greater temporal variability. For example, COM11 (Thiruvalluvar Nagar) shifted from the warmer half of the thermal hierarchy during the morning to comparatively cooler ranks during the afternoon and evening. Interestingly, WB2 (Gandhi Nagar, Adyar) moved from the cooler half during the morning towards warmer ranks during the evening. Overall, these observations indicate that the thermal hierarchy was not maintained across the three observation periods.

3.2 TEMPORAL VARIABILITY IN THERMAL-STATE THRESHOLDS

Monthly air-temperature thresholds defining group 0 (hottest) and group 7 (coolest) varied across months and observation periods (Figure 8). Group 0 thresholds were consistently highest during the afternoon period (13:00–17:00 hours), exceeding 40°C in March and again during September and October. Morning thresholds remained comparatively lower across the year. However, evening thresholds showed greater month-to-month variability. A similar pattern was observed for group 7, with afternoon thresholds consistently remaining higher and evening thresholds lower. The separation between the group 0 and 7 thresholds also varied across months and observation periods, indicating that the air-temperature ranges represented by the thermal groups were not constant throughout the year.

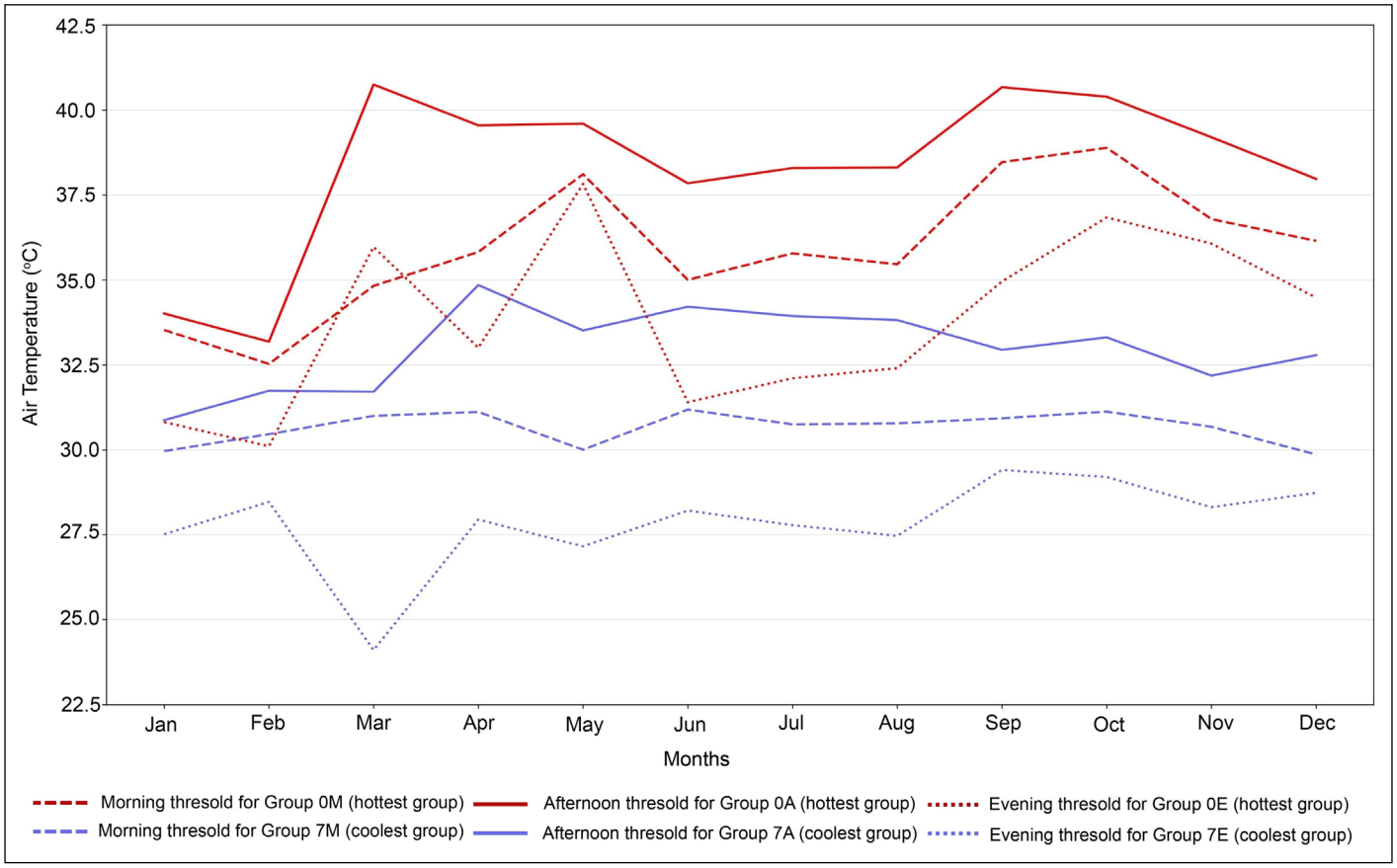

Figure 8: Air temperature-based thermal-state thresholds for classifying study locations (N = 100) by month and observation period, illustrating seasonal and intra-day variation.

3.3 THERMAL-STATE PERSISTENCE AND TRANSITION BEHAVIOUR

Thermal persistence and volatility varied substantially across the study locations (Figure 10). The proportion of transitions remaining within the same thermal domain ranged from approximately 40% to more than 80% (Figure 10). Nearly all locations exhibited cross-domain transitions in at least 25% of total observations. A total of 25% of locations exhibited such transitions in more than 50% of transition instances. MR1C (Nandiambakkam) and ORR4_N (Tirumanam) exhibited the highest persistence and volatility, respectively, and were selected to illustrate contrasting transition behaviour (Figure 9).

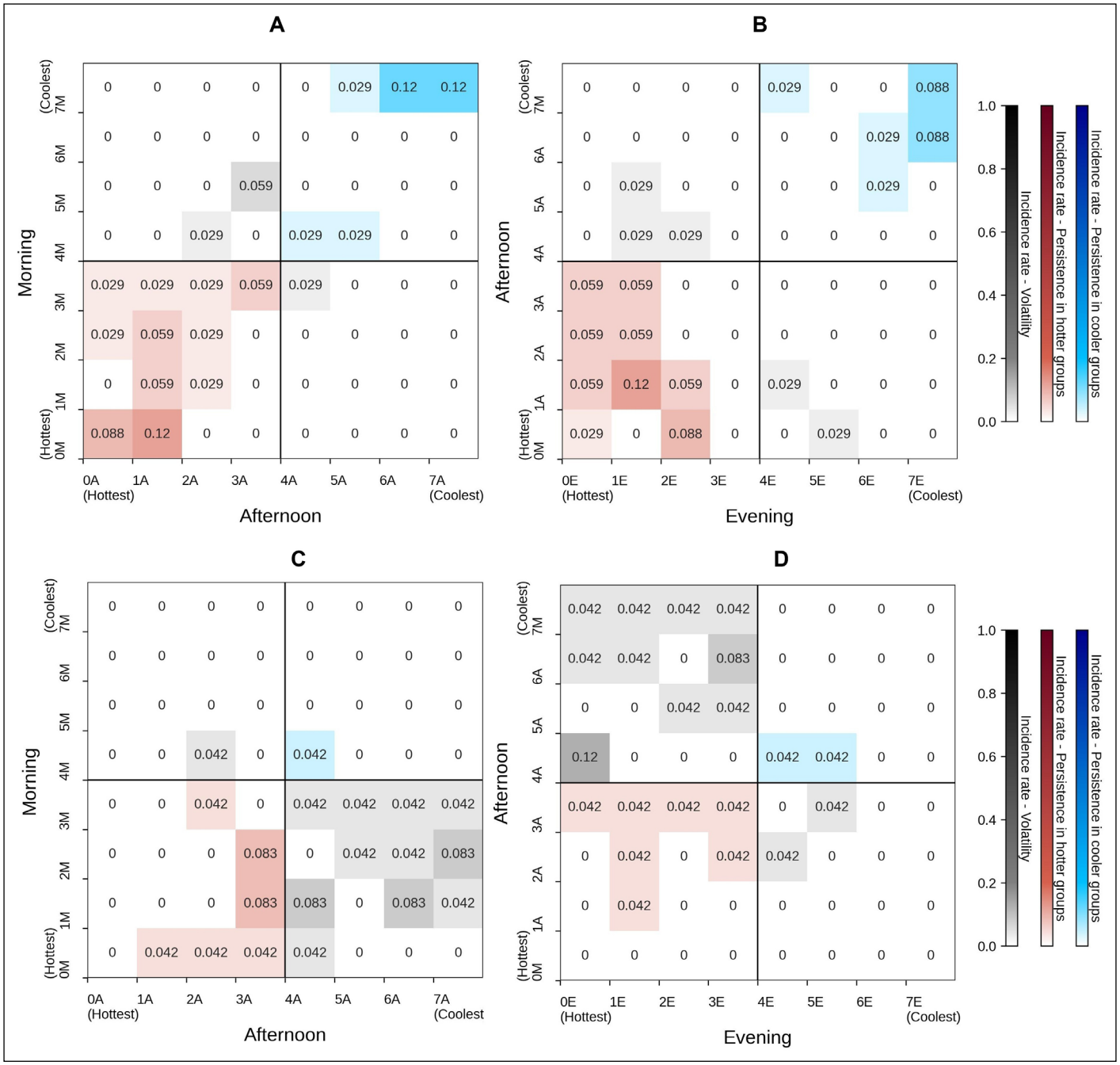

For MR1C, 89% of morning-to-afternoon transitions remained within the same thermal domain, with only 11% occurring between hotter- and cooler-than-peer domains. The highest transition probabilities occurred between group 0 (morning) and group 1 (afternoon) and between group 7 (morning) and group 6 (afternoon), each with a probability of 0.12. A similar pattern was observed for the afternoon-to-evening transitions.

In contrast, ORR4_N exhibited substantially greater thermal volatility. Approximately 63% of morning-to-afternoon transitions occurred between thermal domains. The highest transition probabilities were observed between group 1 (morning) and group 4 (afternoon) and between group 2 (morning) and group 7 (afternoon), each with a probability of 0.083. Afternoon-to-evening transitions also exhibited 63% cross-domain transitions, with the highest probability (0.12) between group 4 (afternoon) and group 0 (evening). Compared with MR1C, transition probabilities were distributed across a wider range of thermal-group combinations.

Figure 9: Thermal-state transition matrices for **(A, B)** MR1C (Nandiambakkam) and **(C, D)** ORR4_N (Tirumanam) showing morning-to-afternoon and afternoon-to-evening transitions.

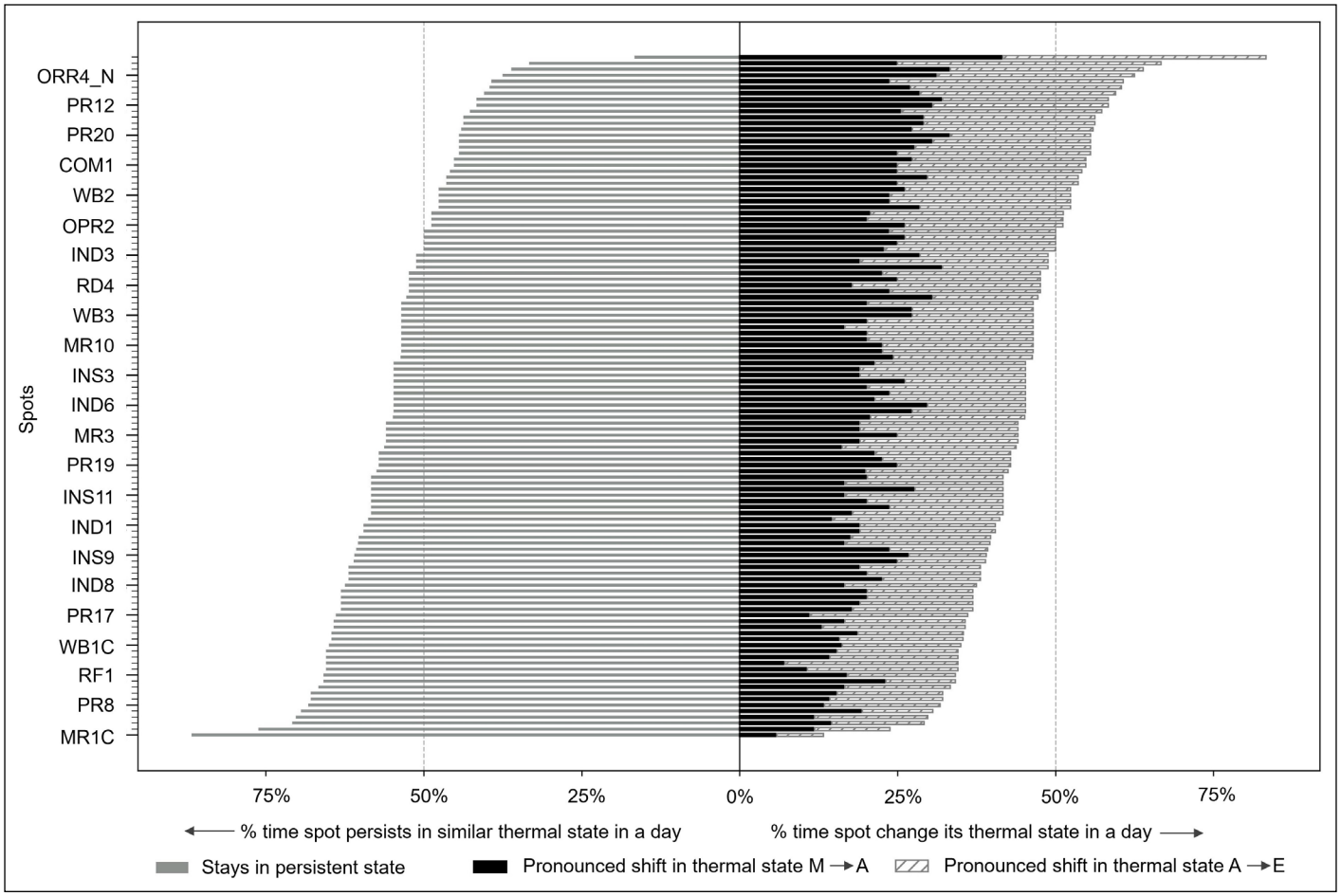

Figure 10: Thermal persistence and thermal-state transition frequencies for 100 study locations across morning (M), afternoon **(A)** and evening **(E)** observation periods.

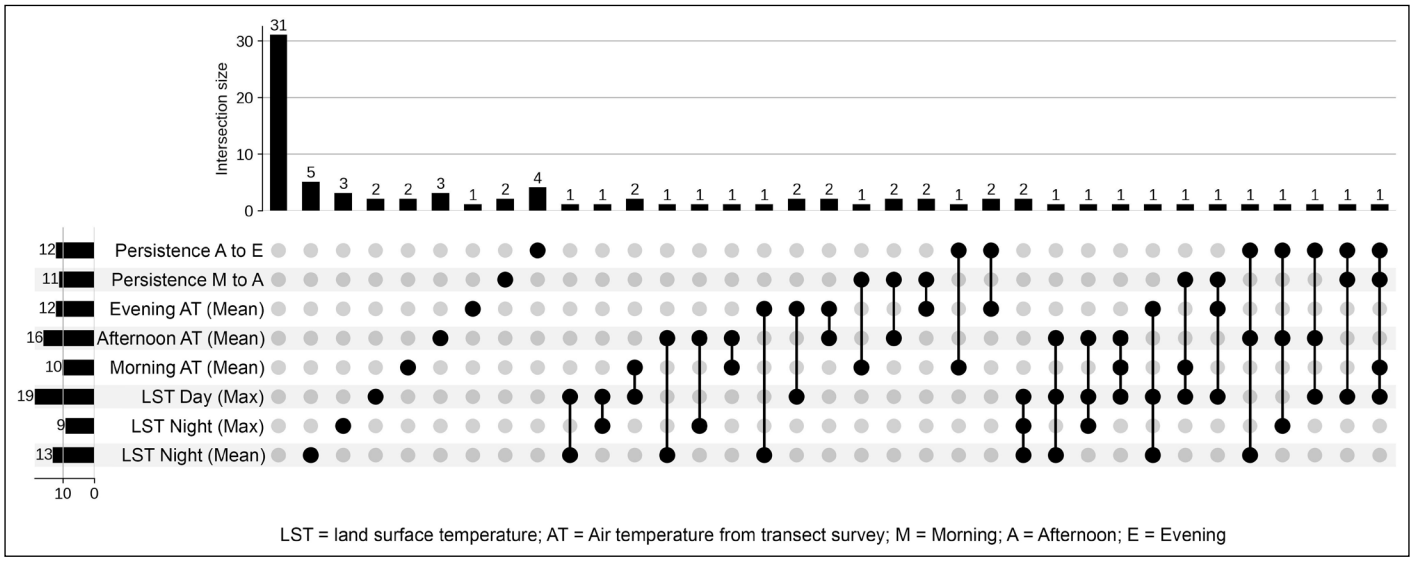

Figure 11: UpSet plot showing intersections among long-term hotspot rankings derived from field-based mean air temperature, satellite-derived day- and night-time land surface temperature (LST) (mean and maximum), and thermal persistence using a ±5 rank-agreement criterion.

Note: AT = air temperature; M = morning; A = afternoon; E = evening.

3.4 VARIABILITY IN HOTSPOT RANKINGS ACROSS THERMAL INDICATORS

The final analysis compared long-term hotspot rankings derived from different thermal indicators for the 86 study locations included in the multi-indicator analysis (Figure 11). The UpSet plot summarises the agreement among these indicator-specific hotspot rankings. A total of 31 study locations (36%) were identified exclusively by the mean daytime LST ranking and were not identified by any other thermal indicator. Agreement between the mean daytime and mean night-time LST rankings was observed for only 13 locations (15%). Similarly, only 13 locations (15%) were jointly identified by three or more thermal indicators. Apart from the daytime LST-specific group, all remaining indicator combinations comprised five or fewer locations, with most containing one to four locations. Thermal persistence did not independently identify hotspot locations but occurred only in combination with one or more field-based air-temperature or satellite-derived LST indicators.

4. DISCUSSION

4.1 TEMPORAL VARIABILITY IN THERMAL HIERARCHY AND CLASSIFICATION

Variation in thermal hierarchy across observation periods indicates that the relative thermal position of study locations is not fixed. Changes in both thermal rankings (Figure 7) and thermal-state classification (Figure 8) indicate that many locations did not maintain the same relative thermal position across the three observation periods. Accordingly, locations identified as hotspots from instantaneous LST-based assessment did not consistently identify locations that remained hot across repeated observations.

These findings are consistent with studies reporting temporal inconsistencies between satellite-derived LST and air temperature observations (Du *et al.* 2023; Sun *et al.* 2020). SUHI and CLUHI assessments exhibit different spatial and temporal behaviour because they are governed by different physical processes (Acosta *et al.* 2023; Du *et al.* 2023; Naserikia *et al.* 2023). Recent studies further show that LST does not accurately represent near-surface thermal conditions (Briegel *et al.* 2025; Zhan *et al.* 2025; Zhao *et al.* 2026). The present findings extend this evidence by demonstrating that hotspots identified from instantaneous LST-based assessment do not consistently remain hot across the intra-day observation period.

4.2 THERMAL PERSISTENCE IN HOTSPOT AND HEATSINK BEHAVIOUR

Thermal persistence varied substantially among the study locations (Figures 9 and 10). The proportion of transitions remaining within the same thermal domain ranged from approximately 40% to more than 80%. While some locations consistently remained hotter or cooler than their peers, others frequently transitioned between thermal domains. These findings indicate that locations assigned to similar thermal states did not necessarily exhibit similar temporal behaviour.

MR1C (Nandiambakkam) and ORR4_N (Tirumanam) illustrate these contrasting behaviours. MR1C exhibited the highest persistence, with 89% of morning-to-afternoon transitions remaining within the same thermal domain, whereas ORR4_N exhibited the highest volatility, with 63% of transitions occurring between hotter- and cooler-than-peer domains. Both locations experienced similar regional meteorological conditions but belonged to different LCZs. Compared with ORR4_N (LCZ 9: sparsely built), MR1C (LCZ 6: open low-rise) has a higher building footprint, lower sky-view factor and lower pervious surface fraction (Stewart & Oke 2012).

These morphological characteristics influence the distribution of net radiation into sensible, latent and storage heat fluxes, producing different thermodynamic responses (Grimmond & Oke 1999; Oke 1982). Higher building footprint and impervious cover increase heat storage potential, whereas greater sky exposure and pervious surfaces enhance radiative cooling, airflow and evapotranspiration (He *et al.* 2020; Oke 1981; Perini & Magliocco 2014). The contrasting temporal behaviour is consistent with established relationships. Thermal persistence therefore complements thermal-state classification by distinguishing locations with similar thermal states but different temporal stability.

The classical definition of LCZs does not accurately represent Indian urban development due to the high degree of heterogeneity in urban characteristics within the standard 400–1000 m horizontal scale (Stewart & Oke 2012). Consequently, relying solely on standard LCZs combined with LST-based thermal mapping may fail to yield effective UHIE mitigation strategies for city retrofitting (Naserikia *et al.* 2023). Instead, a localised, micro-scale evaluation of the urban built environment at approximately 100 m resolution should be adopted alongside thermal condition mapping.

4.3 INFLUENCE OF THERMAL INDICATORS ON HOTSPOT RANKINGS

Hotspot rankings derived from field-based air temperature, day- and night-time LST, and thermal persistence showed limited agreement (Figure 11). A total of 31 locations (36%) were identified exclusively by mean daytime LST, while only 13 locations (15%) were common to both day- and night-time LST rankings. Agreement among three or more indicators was also limited to 13 locations (15%). These results demonstrate that hotspot rankings depend on the thermal indicator adopted in the assessment, as they represent complementary characteristics of the urban thermal environment (Acosta *et al.* 2023; Sun *et al.* 2020; Yang *et al.* 2024). These findings support that UHIE assessment can be strengthened by integrating temporal persistence with conventional thermal indicators to distinguish persistently hot locations from transient hotspots.

5. LIMITATIONS

The study locations were selected based on the literature (Rajagopal *et al.* 2025), which does not account for night-time LST conditions. Data collected across the annual cycle indicate fluctuations that may be attributed to microclimate variations induced by local anthropogenic heat sources, such as traffic-related emissions and heating, ventilation and air-conditioning (HVAC) thermal dissipation from surrounding structures.

The derived thermal groups are based on the measured conditions at these specific locations. While certain locations are labelled as ‘cooler’ in relative terms, they may be hotter in absolute terms. Because this study does not rely on concurrent non-urban thermal conditions, the results describe the relative standing among the monitored locations rather than absolute UHI intensity. Furthermore, the air temperature measurement accuracy (±0.8°C) is close to the 0.5°C standard deviation used to determine the thermal groups. Therefore, the transition between adjacent groups should be interpreted within this specific context.

6. CONCLUSIONS AND NOTES FOR FUTURE STUDIES

This study demonstrates that the temporal characteristics of hotspots are an essential dimension of urban heat island effect (UHIE) assessment. Using one year of repeated air-temperature observations across the Chennai Metropolitan Area (CMA), the analysis showed that hotspot rankings varied across observation periods and according to the thermal indicator adopted, including daytime land surface temperature (LST), night-time LST, air temperature and thermal persistence. These findings indicate that hotspots identified from instantaneous LST-based assessments do not consistently represent locations that remain hot during repeated observations. Thermal persistence distinguishes persistently hot locations from transient hotspots, providing an additional dimension for localised UHIE assessment.

For urban climate researchers, the proposed approach extends conventional hotspot assessment by incorporating temporal characteristics into UHIE evaluation and provides a basis for investigating the processes governing persistent hotspot behaviour. For urban planners, municipal authorities and urban practitioners, it offers an evidence-based approach for prioritising heat-mitigation measures by identifying persistently hot locations. The first generation of heat action plans (HAPs) developed in India to assist the National Disaster Management Authority (NDMA) (2019) and local governments utilised available LST data to determine city-specific mitigation and adaptation measures. While many cities have gained significant experience in managing HAPs and implementing these measures effectively over the last few years, the next iteration of HAPs

may enhance the accuracy of the UHIE assessment. This can be achieved by integrating both LST data and ground observations while accounting for the temporal and persistence behaviour of hotspots. Future research should quantify the physical and morphological controls governing thermal persistence and evaluate the applicability of this assessment framework across diverse climatic regions.

This study provides key insights for future studies by emphasising the need for ground-based measurements that are essential for estimating the UHIE. It also provides crucial guidance on deriving temporal variation in the thermal hierarchy, using Markov-chain analysis of thermal-state transitions, and determining variability in hotspot rankings across thermal indicators. The study also provides an example of how to present key results, as shown in Figure 7 for the temporal mean air temperature distribution across the study location, in Figure 9 for thermal-state transition matrices and in Figure 10 for thermal persistence and thermal-state transition frequencies.

ACKNOWLEDGEMENTS

The authors are grateful to the World Bank, Chennai Metropolitan Development Authority (CMDA) and SRM University for their support in facilitating data collection and providing access to the information essential to this study.

AUTHOR AFFILIATIONS

Rajan Rawal orcid.org/0000-0001-7914-6069
Faculty of Technology, CEPT University, Ahmedabad, IN

Subham Das orcid.org/0009-0006-6354-7064
Faculty of Technology, CEPT University, Ahmedabad, IN

Minu Agarwal orcid.org/0000-0003-3752-875X
Faculty of Technology, CEPT University, Ahmedabad, IN

Tej Chavda orcid.org/0000-0003-1484-0601
Centre for Advanced Research in Building Science and Energy, CEPT University, Ahmedabad, IN

Megh Shah orcid.org/0009-0005-3960-7736
Centre for Advanced Research in Building Science and Energy, CEPT University, Ahmedabad, IN

Stuti Banerjee orcid.org/0009-0005-0046-482X
Centre for Advanced Research in Building Science and Energy, CEPT University, Ahmedabad, IN

Benjamin Hickman orcid.org/0009-0002-1242-9966
Climate Change Division, United Nations Environment Programme (UNEP), New Delhi, IN

R. Shanthi Priya orcid.org/0000-0002-4924-4765
SRM Institute of Science and Technology, Chennai, Tamil Nadu, IN

AUTHOR CONTRIBUTIONS

R.R.: research design, methodology, writing, review and editing; S.D.: data analysis, writing, visualisation; M.A.: methodology, data analysis, review and editing; T.C.: data collection; M.S.: data collection; S.B.: data curation and analysis; B.H.: review and editing; R.S.P.: data collection.

COMPETING INTERESTS

The authors have no competing interests to declare. R.R. is a member of the journal's editorial board, but had no role in, and no influence on, the review and editorial decision processes for this paper.

DATA ACCESSIBILITY

The field measurement data can be accessed by approaching the United Nations Environment Programme (UNEP)—Cool Coalition or Chennai Metropolitan Development Authority (CMDA) Procurement (cmdaprocurement@gmail.com).

FUNDING

The United Nations Environment Programme (UNEP)—Cool Coalition financially supported this study to assist technically the Chennai Metropolitan Development Authority (CMDA), Government of Tamil Nadu, India.

REFERENCES

Acosta, M. P., Vahdatikhaki, F., & **João Santos, A. G. D.** (2023). A comparative analysis of surface and canopy layer urban heat island at the micro level using a data-driven approach. *Sustainable Cities and Society*, 99(December). https://doi.org/10.1016/j.scs.2023.104944

Almeida, C. R., Teodoro, A. C., & **Gonçalves, A.** (2021). Study of the urban heat island (UHI) using remote sensing data/techniques: A systematic review. *Environments*, 8(10), 105. https://doi.org/10.3390/environments8100105

Anna University. (2024a). *Climate risk assessment and adaptation plan of Tamil Nadu: Sustainable habitat*. https://www.annauniv.edu/cccdm/reports/csreports/cssuh.pdf

Anna University. (2024b). *Climate risk assessment and adaptation plan of Tamil Nadu* (Comprehensive Report). https://www.annauniv.edu/cccdm/reports/csreports/cscomprehensive.pdf

Anniballe, R., Bonafoni, S., & **Pichierri, M.** (2014). Spatial and temporal trends of the surface and air heat island over Milan using MODIS data. *Remote Sensing of Environment*, 150, 163–171. https://doi.org/10.1016/j.rse.2014.05.005

Bechtel, B., Alexander, P. J., Böhner, J., Ching, J., Conrad, O., Feddema, J., Mills, G., See, L., & **Stewart, I.** (2015). Mapping local climate zones for a worldwide database of the form and function of cities. *ISPRS International Journal of Geo-Information*, 4(1), 199–219. https://doi.org/10.3390/ijgi4010199

BIS. (2016). *National Building Code of India 2016* (Vols 1–2) (SP 7:2016). Bureau of Indian Standards (BIS). https://bis.gov.in/others/national-building-code/

Branea, A.-M., Danciu, M.-I., Găman, M. S., & **Bădescu, Ş.** (2016, November). Challenges regarding the study of urban heat islands: Ruleset for researchers. Paper presented at the International Conference Risk Reduction for Resilient Cities (RRRC 2016), Bucharest, Romania. https://www.researchgate.net/publication/309740257

Briegel, F., Pinto, J. G., & **Christen, A.** (2025). Is satellite land surface temperature an appropriate proxy for intra-urban variability of daytime heat stress? *Remote Sensing of Environment*, 331(September), 115045. https://doi.org/10.1016/j.rse.2025.115045

Chatzidimitriou, A., & **Yannas, S.** (2017). Street canyon design and improvement potential for urban open spaces; the influence of canyon aspect ratio and orientation on microclimate and outdoor comfort. *Sustainable Cities and Society*, 33(June), 85–101. https://doi.org/10.1016/j.scs.2017.05.019

CMDA. (2008). Spatial strategy and land use planning. In *Second master plan for Chennai Metropolitan Area, 2026* (Vol. 1, pp. 110–118). Chennai Metropolitan Development Authority (CMDA). https://www.cmdachennai.gov.in/Volume1_English_PDF/Vol1_Chapter12_Spatial%20straregy%20and%20LU%20plg.pdf

Demuzere, M., Kittner, J., & **Bechtel, B.** (2021). LCZ Generator: A web application to create local climate zone maps. *Frontiers in Environmental Science*, 9(April). https://doi.org/10.3389/fenvs.2021.637455

Du, H., Zhan, W., Voogt, J., Bechtel, B., Chakraborty, T. C., Liu, Z., Hu, L., Wang, Z., Li, J., Fu, P., Liao, W., & **Luo, M.** (2023). Contrasting trends and drivers of global surface and canopy urban heat islands. *Geophysical Research Letters*, 50(15). https://doi.org/10.1029/2023GL104661

Gabriel, K. R., & **Neumann, J.** (1962). A Markov chain model for daily rainfall occurrence at Tel Aviv. *Quarterly Journal of the Royal Meteorological Society*, 88(375), 90–95. https://doi.org/10.1002/qj.49708837511

Gadekar, K., & **Mathew, A.** (2026). Urban sustainability and disaster risk reduction: Assessing surface urban heat island intensity, thermal hotspots, and land surface temperature trends in Chennai, India. *IFAC Journal of Systems and Control*, 36, 100395. https://doi.org/10.1016/j.ifacsc.2026.100395

Greater Chennai Corporation, Department of Environment and Climate Change, Government of Tamil Nadu, C40 Cities, & **Urban Management Centre.** (2023). *Chennai climate action plan*. https://www.tngcc.tn.gov.in/wp-content/uploads/2025/10/Chennai_Climate_Action_Plan_ENG_5d827c7dec_compressed.pdf

Grimmond, C. S. B., & **Oke, T. R.** (1999). Heat storage in urban areas: Local-scale observations and evaluation of a simple model. *Journal of Applied Meteorology*, 38(7), 922–940. https://doi.org/10.1175/1520-0450(1999)038<0922:HSIUAL>2.0.CO;2

He, B. J., Ding, L., & **Prasad, D.** (2020). Relationships among local-scale urban morphology, urban ventilation, urban heat island and outdoor thermal comfort under sea breeze influence. *Sustainable Cities and Society*, 60, 102289. https://doi.org/10.1016/j.scs.2020.102289

Ho, H. C., Knudby, A., Xu, Y., Hodul, M., & **Aminipouri, M.** (2016). A comparison of urban heat islands mapped using skin temperature, air temperature, and apparent temperature (Humidex), for the Greater Vancouver Area. *Science of The Total Environment*, 544, 929–938. https://doi.org/10.1016/j.scitotenv.2015.12.021

Huang, X., & **Wang, Y.** (2019). Investigating the effects of 3D urban morphology on the surface urban heat island effect in urban functional zones by using high-resolution remote sensing data: A case study of Wuhan, Central China. *ISPRS Journal of Photogrammetry and Remote Sensing*, 152(April), 119–131. https://doi.org/10.1016/j.isprsjprs.2019.04.010

Islam, S., Karipot, A., Bhawar, R., Sinha, P., Kedia, S., & **Khare, M.** (2024). Urban heat island effect in India: A review of current status, impact and mitigation strategies. *Discover Cities*, 1(1). https://doi.org/10.1007/s44327-024-00033-3

Jaiswal, N., Deb, S. K., Panda, S. K., Mandal, A. K., Khan, A. W., & **Kishtawal, C. M.** (2023). Estimation of intra-urban thermal variability in Ahmedabad city using moving vehicle transects. *Journal of Earth System Science*, 132(1). https://doi.org/10.1007/s12040-023-02063-8

Jeganathan, A., Andimuthu, R., Prasannavenkatesh, R., & **Kumar, D. S.** (2016). Spatial variation of temperature and indicative of the urban heat island in Chennai Metropolitan Area, India. *Theoretical and Applied Climatology*, 123(1–2), 83–95. https://doi.org/10.1007/s00704-014-1331-8

Johansson, E., Thorsson, S., Emmanuel, R., & **Krüger, E.** (2014). Instruments and methods in outdoor thermal comfort studies—The need for standardization. *Urban Climate*, 10(P2), 346–366. https://doi.org/10.1016/j.uclim.2013.12.002

Katz, R. W., & **Parlange, M. B.** (1998). Overdispersion phenomenon in stochastic modeling of precipitation. *Journal of Climate*, 11(4), 591–601. https://doi.org/10.1175/1520-0442(1998)011<0591:OPISMO>2.0.CO;2

Kesavan, R., Muthian, M., Sudalaimuthu, K., Sundarsingh, S., & **Krishnan, S.** (2021). ARIMA modeling for forecasting land surface temperature and determination of urban heat island using remote sensing techniques for Chennai city, India. *Arabian Journal of Geosciences*, 14(11). https://doi.org/10.1007/s12517-021-07351-5

Kim, S. W., & **Brown, R. D.** (2021). Urban heat island (UHI) variations within a city boundary: A systematic literature review. *Renewable and Sustainable Energy Reviews*, 148(May), 111256. https://doi.org/10.1016/j.rser.2021.111256

Kotharkar, R., & **Bagade, A.** (2018). Evaluating urban heat island in the critical local climate zones of an Indian city. *Landscape and Urban Planning*, 169(June 2017), 92–104. https://doi.org/10.1016/j.landurbplan.2017.08.009

Kotharkar, R., Ramesh, A., & **Bagade, A.** (2018). Urban heat island studies in South Asia: A critical review. *Urban Climate*, 24, 1011–1026. https://doi.org/10.1016/j.uclim.2017.12.006

Kumar, P., Rai, A., Upadhyaya, A., & **Chakraborty, A.** (2022). Analysis of heat stress and heat wave in the four metropolitan cities of India in recent period. *Science of The Total Environment*, 818, 151788. https://doi.org/10.1016/j.scitotenv.2021.151788

Kumari, P., Garg, V., Kumar, R., & **Kumar, K.** (2021). Impact of urban heat island formation on energy consumption in Delhi. *Urban Climate*, 36(April 2020), 100763. https://doi.org/10.1016/j.uclim.2020.100763

Kustas, W. P., & **Norman, J. M.** (2000). Evaluating the effects of subpixel heterogeneity on pixel average fluxes. *Remote Sensing of Environment*, 74(3), 327–342. https://doi.org/10.1016/S0034-4257(99)00081-4

Lee, S., Yoo, C., Son, B., Cho, D., Im, J., & **Chakraborty, T. C.** (2026). Global patterns of urban heat shaped by climate and morphology. *Nature Communications*, 17, 6445. https://doi.org/10.1038/s41467-026-73062-8

Lefevre, A., Malet-Damour, B., Boyer, H., & **Rivière, G.** (2026). From urban heat island to thermal resilience: Lessons from low-cost microclimate monitoring in a small tropical island. *Urban Climate*, 67, 102913. https://doi.org/10.1016/j.uclim.2026.102913

Li, D., Wang, L., Liao, W., Sun, T., Katul, G., Bou-Zeid, E., & **Maronga, B.** (2024a). Persistent urban heat. *Science Advances*, 10(15), 1–9. https://doi.org/10.1126/sciadv.adj7398

Li, J., Yan, Y., & **Stouffs, R.** (2026). Reevaluating the equity of urban green space distribution: A proposed method integrating urban high-temperature hot spots and temporal dimensions. *Building and Environment*, 292, 114274. https://doi.org/10.1016/j.buildenv.2026.114274

Li, Y., Yang, T., Zhao, G., Ma, C., Yan, Y., Xu, Y., Wang, L., & **Wang, L.** (2024b). A systematic review of studies involving canopy layer urban heat island: Monitoring and associated factors. *Ecological Indicators*, 158, 111424. https://doi.org/10.1016/j.ecolind.2023.111424

Li, Z. L., Wu, H., Duan, S. B., Zhao, W., Ren, H., Liu, X., Leng, P., Tang, R., Ye, X., Zhu, J., Sun, Y., Si, M., Liu, M., Li, J., Zhang, X., Shang, G., Tang, B. H., Yan, G., & **Zhou, C.** (2023). Satellite remote sensing of global land surface temperature: Definition, methods, products, and applications. *Reviews of Geophysics*, 61(1), 1–77. https://doi.org/10.1029/2022RG000777

Magyari-Sáska, Z., Horváth, C., Pop, S., & **Croitoru, A. E.** (2024). A new approach for identification and analysis of urban heat island hotspots. *Journal of Settlements and Spatial Planning*, 15(2), 89–96. https://doi.org/10.24193/JSSP.2024.2.01

Mandvikar, K., Kumar, N., Supe, H., Singh, D., Gupta, A., Kumar, P., Meraj, G., Khan, I. D., Kouser, A., Pandey, S. K., & **Avtar, R.** (2024). Evaluating heat health risk in Indian cities: Geospatial and socio-ecological analysis. *World Development Sustainability*, 5(August), 100180. https://doi.org/10.1016/j.wds.2024.100180

Martinez-Soto, A., Vera-Fonseca, M., Valenzuela-Toledo, P., Melillan-Raguileo, A., & **Shupler, M.** (2025). Heat on the move: Contrasting mobile and fixed insights into Temuco's urban heat islands. *Sensors (Basel)*, 25(4). https://doi.org/10.3390/s25041251

Mohan, M., Bhati, S., & **Sati, A. P.** (2022). Urban heat island effect in India: Assessment, impacts, and mitigation. In Khan, A., Akbari, H., Fiorito, F., Mithun, S., & Niyogi, D. (Eds.), *Global urban heat island mitigation* (pp. 199–250). Elsevier. https://doi.org/10.1016/B978-0-323-85539-6.00007-X

Muller, C. L., Chapman, L., Grimmond, C. S. B., Young, D. T., & **Cai, X.** (2013a). Sensors and the city: A review of urban meteorological networks. *International Journal of Climatology*, 33(7), 1585–1600. https://doi.org/10.1002/joc.3678

Muller, C. L., Chapman, L., Grimmond, C. S. B., Young, D. T., & **Cai, X. M.** (2013b). Toward a standardized metadata protocol for urban meteorological networks. *Bulletin of the American Meteorological Society*, 94(8), 1161–1185. https://doi.org/10.1175/BAMS-D-12-00096.1

Naserikia, M., Hart, M. A., Nazarian, N., Bechtel, B., Lipson, M., & **Nice, K. A.** (2023). Land surface and air temperature dynamics: The role of urban form and seasonality. *Science of the Total Environment*, 905(September), 167306. https://doi.org/10.1016/j.scitotenv.2023.167306

NDMA. (2019). *National guidelines for preparation of action plan: Prevention and management of heat wave*. National Disaster Management Authority (NDMA), Government of India. https://ndma.gov.in/sites/default/files/PDF/Guidelines/heatwaveguidelines.pdf

NITI Aayog & **Asian Development Bank.** (2022). *Cities as engines of growth—TA-9508: Strengthening the states for broad based urban development—Executive summary*. https://www.niti.gov.in/sites/default/files/2022-05/Mod_CEOG_Executive_Summary_18052022.pdf

Oke, T. R. (1981). Canyon geometry and the nocturnal urban heat island: Comparisons of scale model and field observations. *Journal of Climatology*, 1, 237–254. https://doi.org/10.1002/joc.3370010304

Oke, T. R. (1982). The energetic basis of the urban heat island. *Quarterly Journal of the Royal Meteorological Society*, 108(455), 1–24. https://doi.org/10.1002/qj.49710845502

Peng, S., Piao, S., Ciais, P., Friedlingstein, P., Ottle, C., Bréon, F.-M., Nan, H., Zhou, L., & **Myneni, R. B.** (2012). Surface urban heat island across 419 global big cities. *Environmental Science & Technology*, 46(2), 696–703. https://doi.org/10.1021/es2030438

Perini, K., & **Magliocco, A.** (2014). Effects of vegetation, urban density, building height, and atmospheric conditions on local temperatures and thermal comfort. *Urban Forestry and Urban Greening*, 13(3), 495–506. https://doi.org/10.1016/j.ufug.2014.03.003

Pesaresi, M., & **Politis, P.** (2023). *GHS-BUILT-S R2023A—GHS built-up surface grid, derived from Sentinel-2 composite and Landsat, multitemporal (1975–2030)*. European Commission, Joint Research Centre (JRC). https://doi.org/10.2905/9F06F36F-4B11-47EC-ABB0-4F8B7B1D72EA

Rajagopal, P., Shanthi Priya, R., & **Sudha, G.** (2025). Spatial characteristics of urban heat Islands: Land use-based assessment using Chennai's second master plan. *Environmental and Sustainability Indicators*, 28(April), 100900. https://doi.org/10.1016/j.indic.2025.100900

Rajagopalan, P. (2021). Urban heat island and mitigation in tropical India. In Enteria, N., Santamouris, M., & Eicker, U. (Eds.), *Advances in 21st century human settlements* (pp. 183–203). Springer Nature. https://doi.org/10.1007/978-981-33-4050-3_9

Rajan, E. H. S., & **Amirtham, L. R.** (2021). Urban heat island intensity and evaluation of outdoor thermal comfort in Chennai, India. *Environment, Development and Sustainability*, 23(11), 16304–16324. https://doi.org/10.1007/s10668-021-01344-w

Rawat, M., & **Singh, R. N.** (2022). A study on the comparative review of cool roof thermal performance in various regions. *Energy and Built Environment*, 3(3), 327–347. https://doi.org/10.1016/j.enbenv.2021.03.001

Santamouris, M. (2015). Regulating the damaged thermostat of the cities—Status, impacts and mitigation challenges. *Energy and Buildings*, 91, 43–56. https://doi.org/10.1016/j.enbuild.2015.01.027

Schwarz, N., Lautenbach, S., & **Seppelt, R.** (2011). Exploring indicators for quantifying surface urban heat islands of European cities with MODIS land surface temperatures. *Remote Sensing of Environment*, 115(12), 3175–3186. https://doi.org/10.1016/j.rse.2011.07.003

Sharma, P., Singh, R., & **Yogeswaran, N.** (2026). Global review of urban heat island research across varied climatic regions. *Discover Environment*, 4(1), 84. https://doi.org/10.1007/s44274-026-00571-0

Shi, H., Xian, G., Auch, R., Gallo, K., & **Zhou, Q.** (2021). Urban heat island and its regional impacts using remotely sensed thermal data—A review of recent developments and methodology. *Land*, 10(8). https://doi.org/10.3390/land10080867

Sobrino, J. A., Oltra-Carrió, R., Sòria, G., Bianchi, R., & **Paganini, M.** (2012). Impact of spatial resolution and satellite overpass time on evaluation of the surface urban heat island effects. *Remote Sensing of Environment*, 117, 50–56. https://doi.org/10.1016/j.rse.2011.04.042

Sola-Caraballo, J., Serrano-Jiménez, A., Rivera-Gomez, C., & **Galan-Marin, C.** (2025). Multi-criteria assessment of urban thermal hotspots: A GIS-based remote sensing approach in a Mediterranean climate city. *Remote Sensing*, 17(2), 231. https://doi.org/10.3390/rs17020231

Stewart, I. D., & **Oke, T. R.** (2012). Local climate zones for urban temperature studies. *Bulletin of the American Meteorological Society*, 93(12), 1879–1900. https://doi.org/10.1175/BAMS-D-11-00019.1

Stumpe, B., Treptow, J., & **Marschner, B.** (2026). Hot roofs, cool canopies, and hidden streets: Subpixel thermal heterogeneity limits interpretability of satellite-derived LST in urban heat studies. *SSRN*. https://doi.org/10.2139/ssrn.6462447

Sun, T., Sun, R., & **Chen, L.** (2020). The trend inconsistency between land surface temperature and near surface air temperature in assessing Urban heat island effects. *Remote Sensing*, 12(8). https://doi.org/10.3390/RS12081271

Venter, Z. S., Chakraborty, T., & **Lee, X.** (2026). Crowdsourced air temperatures contrast satellite measures of the urban heat island and its mechanisms. *Science Advances*, 7(22), eabb9569. https://doi.org/10.1126/sciadv.abb9569

Voogt, J. A., & **Oke, T. R.** (2003). Thermal remote sensing of urban climates. *Remote Sensing of Environment*, 86(3), 370–384. https://doi.org/10.1016/S0034-4257(03)00079-8

Wang, J., Zhou, W., & **Jiao, M.** (2022). Location matters: planting urban trees in the right places improves cooling. *Frontiers in Ecology and the Environment*, 20(3), 147–151. https://doi.org/10.1002/fee.2455

Weng, Q. (2009). Thermal infrared remote sensing for urban climate and environmental studies: Methods, applications, and trends. *ISPRS Journal of Photogrammetry and Remote Sensing*, 64(4), 335–344. https://doi.org/10.1016/j.isprsjprs.2009.03.007

Wilks, D. S. (2011). Review of probability. In Wilks, D. S. (Ed.), *Statistical methods in the atmospheric sciences* (3rd ed., pp. 7–19). Academic Press. https://doi.org/10.1016/B978-0-12-385022-5.00002-6

WMO. (2023). *Guidance on measuring, modelling and monitoring the canopy layer urban heat island (CL-UHI)* (Report No. 1292). World Meteorological Organization (WMO). https://library.wmo.int/records/item/58410-guidance-on-measuring-modelling-and-monitoring-the-canopy-layer-urban-heat-island-cl-uhi

WMO. (2024). *Guide to instruments and methods of observation*, Vol. 1: *Measurement of meteorological variables* (2024 ed.) (Report No. 8). World Meteorological Organization (WMO). https://library.wmo.int/records/item/68695-guide-to-instruments-and-methods-of-observation

World Bank. (2025). *Towards resilient and prosperous cities in India*. https://documents.worldbank.org/en/publication/documents-reports/documentdetail/099052225091510119

World Bank. (2026). *Urban land area (sq. km)*. https://data.worldbank.org/indicator/AG.LND.TOTL.UR.K2?locations=IN

Yang, Q., Xu, Y., Wen, D., Hu, T., Chakraborty, T. C., Liu, Y., & **Yao, R.** (2024). Satellite clear-sky observations overestimate surface urban heat islands in humid cities. *Geophysical Research Letters*, 51(2). https://doi.org/10.1029/2023GL106995

Zhan, W., Bechtel, B., Du, H., Chakraborty, T., Kotthaus, S., Krayenhoff, S., Martilli, A., Naserikia, M., Nazarian, N., Roth, M., Sismanidis, P., Stewart, I. D., & **Voogt, J.** (2025). Satellite-derived land surface temperatures strongly mischaracterise urban heat hazard. *ArXiv*, 1–24. https://arxiv.org/abs/2509.16568

Zhao, L., Fan, X., & **Hong, T.** (2025). Urban heat island effect: Remote sensing monitoring and assessment—Methods, applications, and future directions. *Atmosphere*, 16(7), 791. https://doi.org/10.3390/atmos16070791

Zhao, L., Zhang, Y., Chakraborty, T., Mazumdar, P., Zhang, K., & **Gentine, P.** (2026). Transfer learning reveals large discrepancies between air and land surface temperatures in cities. *Nature Communications*. https://doi.org/10.21203/rs.3.rs-6665951/v1

Zhou, D., Xiao, J., Bonafoni, S., Berger, C., Deilami, K., Zhou, Y., Frolking, S., Yao, R., Qiao, Z., & **Sobrino, J. A.** (2019). Satellite remote sensing of surface urban heat islands: Progress, challenges, and perspectives. *Remote Sensing*, 11(1), 48. https://doi.org/10.3390/rs11010048

TO CITE THIS ARTICLE:
Rawal, R., Das, S., Agarwal, M., Chavda, T., Shah, M., Banerjee, S., Hickman, B., & Shanthi Priya, R. (2026). Temporal characteristics-based urban heat island effect assessment. *Buildings and Cities*, 7(1), pp. 1375–1396. DOI: https://doi.org/10.5334/bc.901

Submitted: 18 July 2026
Accepted: 31 October 2026
Published: 26 November 2026

COPYRIGHT:
© 2026 The Author(s). This is an open-access article distributed under the terms of the Creative Commons Attribution 4.0 International License (CC-BY 4.0), which permits unrestricted use, distribution, and reproduction in any medium, provided the original author and source are credited. See https://creativecommons.org/licenses/by/4.0/.

Buildings and Cities is a peer-reviewed open access journal published by Ubiquity Press.